SIAM J. NUMER. ANAL.
Vol. 52, No. 4, pp. 2163–2182

A SECOND-ORDER MAXIMUM PRINCIPLE PRESERVING LAGRANGE FINITE ELEMENT TECHNIQUE FOR NONLINEAR SCALAR CONSERVATION EQUATIONS*

JEAN-LUC GUERMOND†, MURTAZO NAZAROV†, BOJAN POPOV†, AND YONG YANG†

Abstract. This paper proposes an explicit, (at least) second-order, maximum principle satisfying, Lagrange finite element method for solving nonlinear scalar conservation equations. The technique is based on a new viscous bilinear form introduced in Guermond and Nazarov [*Comput. Methods Appl. Mech. Engrg.*, 272 (2014), pp. 198–213], a high-order entropy viscosity method, and the Boris–Book–Zalesak flux correction technique. The algorithm works for arbitrary meshes in any space dimension and for all Lipschitz fluxes. The formal second-order accuracy of the method and its convergence properties are tested on a series of linear and nonlinear benchmark problems.

Key words. conservation equations, parabolic regularization, entropy, limiters, entropy solutions, finite element method

AMS subject classifications. 65M60, 35L65

DOI. 10.1137/130950240

1. Introduction.

Imposing both the maximum principle and high-order accuracy in space is a difficult task for numerical methods approximating scalar conservation equations. The Godunov theorem even asserts that it is impossible for one-step linear approximation methods to be at least second-order accurate in space and be monotonicity preserving. Satisfying the maximum principle and having high-order accuracy on arbitrary meshes in any space dimension are very desirable properties in all applications, but these are two contradicting requirements: (i) on one hand one needs to add artificial viscosity to guarantee the maximum principle; (ii) on the other hand one needs to stay as close as possible to the Galerkin discretization of the problem to be high-order accurate in space. Enforcing the maximum principle using finite volume methods with piecewise constant approximation goes back to the early works of Lax and Godunov. Constructing second-order (or higher-order) maximum principle preserving methods by making use of limiting techniques in one space dimension or on uniform Cartesian grids in higher space dimensions is also well known; see, for example, Boris and Book [3], Zalesak [33], Sanders [29], Liu [25], Nessyahu and Tadmor [27], and Jiang and Tadmor [19] for finite volume methods, and Zhang and Shu [34], Zhang, Xia, and Shu [35], and Zhang, Zhang, and Shu [36] for the discontinuous Galerkin methods. Extensions to nonuniform finite volumes are also known; see, e.g., Piar et al. [28]. Quite surprisingly, the general case of continuous finite elements on unstructured meshes in arbitrary space dimension is not yet fully understood. Although interesting and effective nonlinear stabilization techniques and limiting strategies have been proposed for finite elements (see, e.g., Burman and Ern

*Received by the editors December 23, 2013; accepted for publication (in revised form) June 17, 2014; published electronically August 19, 2014. The research of the authors was supported in part by the National Science Foundation grants DMS-1015984 and DMS-1217262, by the Air Force Office of Scientific Research, USAF, under grant/contract FA99550-12-0358, and by Award KUS-C1-016-04, made by King Abdullah University of Science and Technology (KAUST).

http://www.siam.org/journals/sinum/52-4/95024.html

†Department of Mathematics, Texas A&M University, 3368 TAMU, College Station, TX 77843 (guermond@math.tamu.edu, murtazo@math.tamu.edu, popov@math.tamu.edu, yytamu@gmail.com). The first author is on leave from CNRS, France.

[5], Burman and Ern [6], Burman [4], and Badia and Hierro [1] for nonlinear viscosities, and Kuzmin [22] and Kuzmin and Turek [24] for limiters), until recently there did not exist in the literature an explicit, first-order, continuous finite element method with linear viscosity that could be proven to satisfy the maximum principle on any mesh (e.g., irrespective of any angle condition), in any space dimension, and with any Lipschitz flux. To the best of our knowledge, the first method with these properties has been constructed in Kuzmin and Turek [24] using an edge-based viscosity and in Guermond and Nazarov [13] using an element-based viscosity. The goal of the present paper is to extend the first-order technique introduced in [13] to an explicit second-order maximum principle preserving numerical method that works on arbitrary meshes in any space dimension with any Lipschitz flux using continuous Lagrange finite elements. The four key ingredients are the first-order technique [13], a novel treatment of the consistent mass matrix by Guermond and Pasquetti [16], a high-order technique (entropy-viscosity method of Guermond, Pasquetti, and Popov [17]), and the Boris–Book–Zalesak flux correction technique [3, 33]. The main characteristics of the new method are (i) it is maximum principle preserving, (ii) it preserves the accuracy of the entropy viscosity method, and (iii) the dispersion errors induced by mass lumping are corrected in the flux limiting step.

The paper is organized as follows. Preliminary technicalities and the construction of the first-order viscosity, which is the starting point for building the higher-order algorithm, are described in section 2. The full description of the method, including time and space discretization and limiting, is given in section 3. The novel correction technique that counteracts the dispersive effects of mass lumping is described in section 3.3. The adaptation of the Boris–Book–Zalesak flux correction technique to the present setting is done in section 3.4. The main result of the paper is Theorem 3.6. The convergence behavior of the new method is investigated in section 4. The key steps of the limiting process, which is based on the Boris–Book–Zalesak flux correction technique, are recalled in the Appendix A.

2. Preliminaries. In this section, the problem is formulated, the finite element setting is introduced, some key shortcomings of the traditional notion of isotropic artificial viscosity are listed, and a novel definition of a first-order artificial viscosity introduced in Guermond and Nazarov [13] is recalled.

2.1. Formulation of the problem. Let Ω be an open polyhedral domain in $\mathbb{R}^d$, d being the space dimension. Let $\boldsymbol{f} \in \mathrm{Lip}(\mathbb{R};\mathbb{R}^d)$ be a vector-valued function that we hereafter call flux, and let $u_0 \in L^\infty(\Omega)$ be some initial data. We consider the scalar-valued conservation equations

$$\partial_t u + \nabla\cdot\boldsymbol{f}(u) = 0, \qquad u(\boldsymbol{x},0) = u_0(\boldsymbol{x}), \quad (\boldsymbol{x},t) \in \Omega\times\mathbb{R}_+. \tag{2.1}$$

To simplify questions regarding boundary conditions, we assume that either periodic boundary conditions are enforced or the initial data is compactly supported, and in that case we are interested in the solution before the domain of influence of u_0 reaches the boundary of Ω. This problem has a unique entropy solution satisfying the additional entropy inequalities $\partial_t E(u) + \nabla\cdot\boldsymbol{F}(u) \le 0$ for all convex entropies $E \in \mathrm{Lip}(\mathbb{R};\mathbb{R})$ and associated entropy fluxes $\boldsymbol{F}_i(u) = \int_0^u E'(v)\boldsymbol{f}_i'(v)\,\mathrm{d}v$, $1 \le i \le d$ (see Kružkov [20] and Bardos, le Roux, and Nédélec [2]).

2.2. Mesh. Let $\{\mathcal{K}_h\}_{h>0}$ be a mesh family that we assume to be affine, conforming (no hanging nodes), and shape-regular in the sense of Ciarlet. By convention, the elements in $\mathcal{K}_h$ are closed in $\mathbb{R}^d$. We may have different reference elements, but always

finitely many. For example, the mesh $\mathcal{K}_h$ could be composed of a mixture of triangles and quadrangles in two space dimensions, or composed of a mixture of tetrahedra, hexahedra, and prisms in three space dimensions. The reference elements are denoted $\widehat{K}$, and the affine diffeomorphism mapping $\widehat{K}$ to an arbitrary element $K \in \mathcal{K}_h$ is denoted $\Phi_K : \widehat{K} \longrightarrow K$.

Our objective is to approximate the entropy solution of (2.1) with H^1-conforming finite elements. To this end we define the scalar-valued Lagrange finite element approximation space

$$X_h = \{v \in \mathcal{C}^0(\Omega;\mathbb{R});\, v|_K \circ \Phi_K \in Q \ \forall K \in \mathcal{K}_h\}, \tag{2.2}$$

where Q is a polynomial space that depends on the reference element $\widehat{K}$.

Let $\{\varphi_1,\dots,\varphi_N\}$ be the nodal Lagrange basis associated with the Lagrange nodes of the mesh $\mathcal{K}_h$, say, $\{\boldsymbol{a}_1,\dots,\boldsymbol{a}_N\}$, i.e., $\varphi_i(\boldsymbol{a}_j) = \delta_{ij}$. We denote by S_i the support of φ_i and by $|S_i|$ the measure of S_i, $i = 1,\dots,N$. We also define $S_{ij} := S_i \cap S_j$ as the intersection of the two supports S_i and S_j. Let E be a union of cells in $\mathcal{K}_h$; we define $\mathcal{I}(E) := \{j \in \{1,\dots,N\};\, |S_j \cap E| \neq 0\}$ as the set that contains the indices of all the shape functions whose support on E is of nonzero measure.

Note that the polynomial degree of the approximation is unspecified, but it is essential to assume that X_h is such that the mass matrix can be lumped and the lumped mass matrix is positive definite. We formalize this hypothesis by introducing the following notation and assumption for all $K \in \mathcal{K}_h$:

$$0 < \mu_K^{\min} := \min_{i\in\mathcal{I}(K)} \frac{1}{|K|}\int_K \varphi_i(\boldsymbol{x})\,\mathrm{d}\boldsymbol{x}, \quad \mu_K^{\max} := \max_{i\in\mathcal{I}(K)} \frac{1}{|K|}\int_K |\varphi_i(\boldsymbol{x})|\,\mathrm{d}\boldsymbol{x}. \tag{2.3}$$

Let n_K be the number of vertices in K, i.e., $n_K = \mathrm{card}(\mathcal{I}(K))$. Owing to the mesh being affine, the quantities $\mu_K^{\min}$, $\mu_K^{\max}$, and n_K depend only on $\widehat{K}$. Since the number of reference elements defining the mesh family is finite, we now define

$$\lambda := \max_{\mathcal{K}_h} \max_{K\in\mathcal{K}_h} \frac{\mu_K^{\max}}{\mu_K^{\min}} < +\infty. \tag{2.4}$$

Note that $\lambda = 1$ for any discrete setting with nonnegative shape functions—for example, $\mathbb{P}_1$ approximation on simplices.

We define the local minimum mesh size h_K for any $K \in \mathcal{K}_h$ as

$$h_K := \frac{1}{\max_{i\in\mathcal{I}(K)} \|\nabla\varphi_i\|_{L^\infty(K)}} \tag{2.5}$$

and the global minimum mesh size as $h := \min_{K\in\mathcal{K}_h} h_K$. The parameters h and λ are used to define the CFL number (see Theorem 3.1).

2.3. Viscosity bilinear form. It has been shown in Guermond and Nazarov [13] that the viscosity bilinear form based on the operator $-\nabla\cdot(\nu_h(u)\nabla)$, where $\nu_h(u)$ is scalar-valued, fails in general to guarantee the maximum principle. In particular, this form is not robust with respect to the shape of the cells. For instance, it fails if the mesh does not satisfy the so-called acute angle condition assumption; see, e.g., Burman and Ern [5, Eq. (8)]. Moreover, the traditional definition of $\nu_h(u)$ is somewhat questionable. For instance, using some one-dimensional argument based on uniform grids, it is usual to take $\nu_h(u) = c_M\|\boldsymbol{f}'\|_{L^\infty}h$, where c_M is a user-defined constant and h is the meshsize. One important question that then immediately arises in two and

higher-space dimensions is that of a proper definition of the meshsize h on nonuniform anisotropic meshes. Although many clever and reasonably well-justified ideas have been proposed to address this nontrivial issue (see, e.g., Tezduyar and Osawa [31], Tezduyar and Sathe [30], Campbell and Shashkov [7], and Dobrev, Kolev, and Rieben [10]), to the best of our knowledge, none of them have yet led to a provable maximum principle holding for every nonlinear flux $\boldsymbol{f} \in \mathrm{Lip}(\mathbb{R}, \mathbb{R}^d)$ and every mesh, even for piecewise linear approximation. Once some meshsize h has been chosen, one then runs into the problem of choosing the constant c_M that multiplies $h\|\boldsymbol{f}'\|_{L^\infty}$ to form the viscosity. Although $c_M = \frac{1}{2}$ seems to be a reasonable choice justified by the one-dimensional analysis on uniform meshes, we do not know of any rationale for tuning this constant in two and three space dimensions on arbitrary grids besides heuristic arguments and trial-and-error tests. Again, even though it is possible to establish well-founded heuristic arguments to tune the constant (see, e.g., Tezduyar and Osawa [31], Tezduyar and Sathe [30], and Guermond, Pasquetti, and Popov [17]), we do not know of any argument yielding a provable maximum principle for every nonlinear flux $\boldsymbol{f}$ and every mesh.

As proposed in Guermond and Nazarov [13], we abandon in this paper the PDE-based definition of the viscosity (i.e., $-\nabla\cdot(\nu_h(u)\nabla)$) and adopt instead a graph-theoretic approach. Let K be a cell in $\mathcal{K}_h$; an artificial viscosity bilinear form is defined on K following the key properties identified in Guermond and Nazarov [13]:

1. $b_K(\varphi_j, \varphi_i) = 0$ if $i \notin \mathcal{I}(K)$ or $j \notin \mathcal{I}(K)$,
2. $b_K(\varphi_j, \varphi_i) \sim -|K|$ if $i \neq j$, $i, j \in \mathcal{I}(K)$,
3. symmetry $b_K(\varphi_j, \varphi_i) = b_K(\varphi_i, \varphi_j)$,
4. conservation $\sum_{j\neq i} b_K(\varphi_i, \varphi_j) = -b_K(\varphi_i, \varphi_i)$.

Recalling that $n_K := \mathrm{card}(\mathcal{I}(K))$, we define $\rho := \min_{K\in\mathcal{K}_h} \frac{1}{n_K-1}$. Then the local bilinear form b_K defined as follows satisfies all the above requirements:

$$b_K(\varphi_j, \varphi_i) = \begin{cases} -\frac{1}{n_K-1}|K| & \text{if } i \neq j, \quad i, j \in \mathcal{I}(K), \\ |K| & \text{if } i = j, \quad i, j \in \mathcal{I}(K), \\ 0 & \text{if } i \notin \mathcal{I}(K) \text{ or } j \notin \mathcal{I}(K). \end{cases} \tag{2.6}$$

The global artificial viscosity bilinear form is then defined as

$$b(u_h, v_h) = \sum_{K\in\mathcal{K}_h} \sum_{i,j\in\mathcal{I}(K)} \nu_K U_j V_i b_K(\varphi_j, \varphi_i), \tag{2.7}$$

where $u_h(\boldsymbol{x}, t) = \sum_{i=1}^N U_i(t)\varphi_i(\boldsymbol{x})$, $v_h = \sum_{i=1}^N V_i\varphi_i$, and ν_K is a viscosity constant yet to be defined on each cell. Therefore, the semidiscretized and stabilized form of problem (2.1) consists of finding $u_h \in \mathcal{C}^1([0, T]; X_h)$ so that the following holds for any $v_h \in X_h$:

$$\int_\Omega (\partial_t u_h + \nabla\cdot\boldsymbol{f}(u_h))v_h \,\mathrm{d}\boldsymbol{x} + b(u_h, v_h) = 0. \tag{2.8}$$

Remark 2.1. It is shown in Guermond and Nazarov [13] that

$$b_K(\varphi_j, \varphi_i) = \kappa \int_K \mathbb{J}^{\mathsf{T}}(\nabla\varphi_j)\cdot\mathbb{J}^{\mathsf{T}}(\nabla\varphi_i),$$

where $\mathbb{J}$ is the Jacobian matrix of the geometric transformation $\Phi_K : \widehat{K} \longrightarrow K$ when K is a simplex and the shape functions are piecewise linear. In this case $\kappa = \frac{4}{3}$ in two space dimensions and $\kappa = \frac{3}{2}$ in three space dimensions, and the effective viscosity, in the traditional sense, is the tensor $\kappa\nu_K\mathbb{J}\mathbb{J}^{\mathsf{T}}$.

3. Space and time approximation. We introduce in this section the time approximation of (2.8), and we define the piecewise constant viscosity field ν_K. We introduce in section 3.1 the first-order explicit Euler time stepping and a first-order viscosity that guarantees the maximum principle. This technique is then extended to higher order in space and time in section 3.2.

3.1. First-order viscosity. Let $u_{0h} \in X_h$ be an approximation of u_0 that satisfies the discrete maximum principle, i.e.,

$$u_{\min} := \inf_{\boldsymbol{x}\in\Omega} u_0(\boldsymbol{x}) \le \min_{1\le i\le N} u_{0h}(\boldsymbol{a}_i) \le \max_{1\le i\le N} u_{0h}(\boldsymbol{a}_i) \le \sup_{\boldsymbol{x}\in\Omega} u_0(\boldsymbol{x}) := u_{\max}. \tag{3.1}$$

In order to define a CFL number, we need to estimate the maximum wave speed. First we define the following subset of X_h:

$$B_h = \{v_h \in X_h \mid u_{\min} \le \min_{1\le i\le N} v_h(\boldsymbol{a}_i) \le \max_{1\le i\le N} v_h(\boldsymbol{a}_i) \le u_{\max}\}. \tag{3.2}$$

It can be shown that

$$u^*_{\min} := \inf_{\{\mathcal{K}_h\}_{h>0}} \inf_{v_h\in B_h,\ \boldsymbol{x}\in\Omega} v_h(\boldsymbol{x}) \quad \text{and} \quad u^*_{\max} := \sup_{\{\mathcal{K}_h\}_{h>0}} \sup_{v_h\in B_h} \sup_{\boldsymbol{x}\in\Omega} v_h(\boldsymbol{x}) \tag{3.3}$$

are finite; in particular, there are constants $c_{\min}$ and $c_{\max}$ that depend only on the collection of reference finite elements $\{(\widehat{K}, \widehat{P}, \widehat{\Sigma})\}$, such that $c_{\min}u_{\min} \le u^*_{\min}$ and $u^*_{\max} \le c_{\max}u_{\max}$. We then define the maximum wave speed to be

$$\beta := \sup_{v\in[u^*_{\min},u^*_{\max}]} \|\boldsymbol{f}'(v)\|. \tag{3.4}$$

Let $t^n \ge 0$ be the current time, and let $\Delta t^n > 0$ be the current time step; i.e., $t^{n+1} = t^n + \Delta t^n$. Let $u_h^n := \sum_{j=1}^N U_j^n \varphi_j \in X_h$ be the approximation of $u(\cdot, t^n)$. The nodal values of the low-order solution $u_{h,L}^{n+1} = \sum_{j=1}^N U_{L,j}^{n+1}\varphi_j \in X_h$ at time t^{n+1} are evaluated as follows:

$$U_{L,i}^{n+1} = U_i^n - \Delta t^n m_i^{-1} \sum_{K\subset S_i} \left(\nu_K^{L,n} b_K(u_h^n, \varphi_i) + \int_K \nabla\cdot(\boldsymbol{f}(u_h^n))\varphi_i \,\mathrm{d}\boldsymbol{x} \right), \tag{3.5}$$

where the mass matrix is lumped and $m_i := \int_{S_i} \varphi_i \,\mathrm{d}\boldsymbol{x}$. Following Guermond and Nazarov [13], the piecewise constant viscosity field is defined as follows on each cell $K \in \mathcal{K}_h$:

$$\nu_K^{L,n} = \max_{i\ne j\in\mathcal{I}(K)} \frac{\max\left(0, \int_{S_{ij}} (\boldsymbol{f}'(u_h^n)\cdot\nabla\varphi_j)\varphi_i \,\mathrm{d}\boldsymbol{x}\right)}{\sum_{T\subset S_{ij}} -b_T(\varphi_j,\varphi_i)}. \tag{3.6}$$

The lower index L in $U_{L,i}^{n+1}$ and the upper index L in $\nu_K^{L,n}$ refer to the low-order method. The justification for the above definition of $\nu_K^{L,n}$ is the following result.

THEOREM 3.1 (Guermond and Nazarov [13]). *In addition to the above assumptions on the mesh-family and on the flux, assume that the CFL number* $\frac{\beta\Delta t^n}{h}$ *is such that* $\frac{\beta\Delta t^n}{h} \le \frac{1}{\lambda(1+\rho^{-1})}$. *Then the solution to* (3.5) *satisfies the local discrete maximum principle; i.e.,* $u_{\min} \le \min_{j\in\mathcal{I}(S_i)} U_j^n \le U_{L,i}^{n+1} \le \max_{j\in\mathcal{I}(S_i)} U_j^n \le u_{\max}$ *for all* $n \ge 0$.

COROLLARY 3.2. *Under the assumptions of Theorem* 3.1*, the solution to* (3.5) *satisfies the following* L^∞*-estimates:*

$$c_{\min}u_{\min} \le u_h^n(\boldsymbol{x}) \le c_{\max}u_{\max} \quad \forall n \ge 0,\ \forall \boldsymbol{x} \in \Omega. \tag{3.7}$$

Moreover, if the space X_h is such that $\min_{\ell\in\mathcal{I}(K)} v(\boldsymbol{a}_\ell) \le v(\boldsymbol{x}) \le \max_{\ell\in\mathcal{I}(K)} v(\boldsymbol{a}_\ell)$ $\forall v \in X_h$, $\forall \boldsymbol{x} \in K$, $\forall K \in \mathcal{K}_h$, *then the following holds for all* $K \in \mathcal{K}_h$*:*

$$\min_{i\in\mathcal{I}(K)} \min_{j\in\mathcal{I}(S_i)} U_j^n \le u_h^{n+1}(\boldsymbol{x}) \le \max_{i\in\mathcal{I}(K)} \max_{j\in\mathcal{I}(S_i)} U_j^n \quad \forall n \ge 0. \tag{3.8}$$

Remark 3.1 (SSP extension). The result of Theorem 3.1 directly extends to any higher-order strong stability preserving (SSP) time stepping (see, e.g., Gottlieb, Shu, and Tadmor [11] for a review) since each step of any SSP method is a convex combination of solutions of forward Euler substeps. We restrict ourselves in the rest of the paper to the explicit Euler time stepping to simplify the presentation, but everything that is said hereafter in this context regarding the maximum principle extends to SSP methods.

PROPOSITION 3.3 (conservation). *The method is conservative in the sense that* $\int_\Omega u_{h,L}^{n+1}\,d\boldsymbol{x} = \int_\Omega u_h^n\,d\boldsymbol{x}$.

Proof. The definition (3.5) implies that

$$\begin{aligned}\int_\Omega (u_{h,L}^{n+1} - u_h^n)\,\mathrm{d}\boldsymbol{x} &= \sum_{i=1}^N (U_{L,i}^{n+1} - U_i^n) \int_\Omega \varphi_i\,\mathrm{d}\boldsymbol{x} = \sum_{i=1}^N m_i (U_{L,i}^{n+1} - U_i^n)\\ &= -\Delta t^n \sum_{K\subset\mathcal{K}_h} \left(\nu_K^{L,n} b_K\left(u_h^n, \sum_{i=1}^N \varphi_i\right) + \int_K \nabla\cdot(\boldsymbol{f}(u_h^n)) \sum_{i=1}^N \varphi_i\,\mathrm{d}\boldsymbol{x}\right).\end{aligned}$$

Then we conclude by using the partition of unity property $\sum_{i=1}^N \varphi_i = 1$, the conservation property of b_K, $b_K(\varphi_j, \sum_{i=1}^N \varphi_i) = 0$ $\forall j \in \{1,\dots,N\}$, and the assumptions on the boundary conditions. ∎

3.2. High-order viscosity. We now construct a higher-order method using the notion of entropy viscosity introduced in Guermond and Pasquetti [15] and Guermond, Pasquetti, and Popov [17]. Proceeding as in Guermond and Nazarov [13], the higher-order viscosity is defined to be the minimum of the first-order viscosity defined in (3.6) and an entropy residual. Let $E \in \mathrm{Lip}(\mathbb{R};\mathbb{R})$ be a convex entropy. Let K be a cell in the mesh $\mathcal{K}_h$. We define an entropy residual over K as follows:

$$R_K^n(u_h^n, u_h^{n-1}) = \|\tfrac{1}{\Delta t^{n-1}}(E(u_h^n) - E(u_h^{n-1})) + \boldsymbol{f}'(u_h^n)\cdot\nabla E(u_h^n)\|_{L^\infty(K)}. \tag{3.9}$$

The L^∞-norm over K is estimated by evaluating the residual at the quadrature points. A first-order approximation of the time derivative $\partial_t E(u)$ is used here, but a second-order or a higher-order approximation of the derivative of the entropy can easily be constructed. For instance, the computation of the entropy residual can be embedded within Runge–Kutta substeps; we omit the details for simplicity. Let F be a face of K, and assume that F is an interface, i.e., F is not a boundary face. It is useful to evaluate the entropy jump across the cell interfaces

$$J_F^n(u_h) = \|\boldsymbol{f}'(u_h^n)\cdot\boldsymbol{n}[\![\partial_n E(u_h^n)]\!]\|_{L^\infty(F)}. \tag{3.10}$$

Let $\nu_K^{L,n}$ be the first-order viscosity defined in (3.6). The so-called entropy viscosity is constructed as follows:

$$\nu_K^{H,n} = \min\Big(\nu_K^{L,n}, \frac{c_E R_K^n(u_h^n, u_h^{n-1}) + c_J \max_{F\in\partial K} J_F^n(u_h^n)}{\|E(u_h^n) - \overline{E}(u_h^n)\|_{L^\infty(\Omega)}}\Big), \tag{3.11}$$

where c_E and c_J are user-defined parameters of order unity and $\overline{E}(u_h^n)$ is the mean of $E(u_h^n)$ over Ω (the index H refers to high-order). The key improvement over earlier versions of the method (see, e.g., Guermond and Pasquetti [15] and Guermond, Pasquetti, and Popov [17]) is that the definition (3.11) does not invoke any notion of meshsize. All the quantities $\nu_K^{H,n}$, $\nu_K^{L,n}$, R_K^n, J_K^n scale like the inverse of a distance to the square times a wave speed. The method is not yet parameter free due to the presence of c_E and c_J. We have observed that $c_E \sim 1$ and $c_J \sim 1$ make the method work satisfactorily in all the applications we have investigated.

3.3. Mass lumping versus consistent mass matrix. It is well known that lumping the mass matrix induces high dispersion errors, as shown in, e.g., Christon [8], Christon, Martinez, and Voth [9], Gresho, Sani, and Engelman [12], Voth, Martinez, and Christon [32], Kuzmin [22], and Guermond and Pasquetti [16]. A cure for this problem is to use the consistent mass matrix, but it is also known (see, e.g., Guermond and Yang [18]) that the inverse of the consistent mass matrix is not maximum principle preserving. Some remedies to this additional problem have been suggested in Kuzmin [22]. We propose in this section an approach, slightly different from that of Kuzmin [22], based on an idea from Guermond and Pasquetti [16] that leads to a simple and robust algorithm.

Let $\mathcal{M}^C$ and $\mathcal{M}^L$ be the consistent and lumped mass matrices, respectively. The entries of $\mathcal{M}^C$ and $\mathcal{M}^L$ are $\mathcal{M}_{ij}^C := \int_\Omega \varphi_i(\boldsymbol{x})\varphi_j(\boldsymbol{x})\,\mathrm{d}\boldsymbol{x}$ and $\mathcal{M}_{ij}^L := \delta_{ij}\int_\Omega \varphi_i(\boldsymbol{x})\,\mathrm{d}\boldsymbol{x}$, respectively. Upon setting $\mathcal{B} = (\mathcal{M}^L - \mathcal{M}^C)(\mathcal{M}^L)^{-1}$, denoting $\mathcal{I}$ the identity matrix, and observing that $\mathcal{M}^C = (\mathcal{I} - \mathcal{B})\mathcal{M}^L$, the inverse of $\mathcal{M}^C$ can formally be put into the following form:

$$(\mathcal{M}^C)^{-1} = (\mathcal{M}^L)^{-1}(\mathcal{I} + \mathcal{B} + \mathcal{B}^2 + \ldots).$$

The Neumann series can be shown to be convergent. For instance, it is shown in Guermond and Pasquetti [16] that the spectral radius of $\mathcal{B}$ is less than $\frac{3}{4}$ for $\mathbb{P}_1$ Lagrange finite elements in two space dimensions. It is also shown therein that approximating $(\mathcal{M}^C)^{-1}$ by $(\mathcal{M}^L)^{-1}(\mathcal{I} + \mathcal{B})$ exactly corrects the dispersion error induced by mass lumping for $\mathbb{P}_1$ elements.

Denoting $G \in \mathbb{R}^N$ the column vector with entries

$$G_i := \sum_{K\subset S_i}\left(\nu_K^{H,n} b_K(u_h^n,\varphi_i) + \int_K \nabla\cdot(\boldsymbol{f}(u_h^n))\varphi_i\,\mathrm{d}\boldsymbol{x}\right), \tag{3.12}$$

we then define the high-order solution $u_{h,H}^{n+1} := \sum_{i=1}^N U_{H,i}^{n+1}\varphi_i$ as follows:

$$U_H^{n+1} = U^n - \Delta t^n(\mathcal{M}^L)^{-1}(\mathcal{I} + \mathcal{B})G. \tag{3.13}$$

LEMMA 3.4. *The following property holds:* $\sum_{i\in\mathcal{I}(S_j)}\mathcal{B}_{ij} = 0$.

Proof. Using the definition $\mathcal{B} = (\mathcal{M}^L - \mathcal{M}^C)(\mathcal{M}^L)^{-1}$, we have

$$\sum_{i\in\mathcal{I}(S_j)}\mathcal{B}_{ij} = 1 - \sum_{i\in\mathcal{I}(S_j)}\frac{\mathcal{M}_{ij}^C}{m_j} = 1 - \frac{m_j}{m_j} = 0,$$

which completes the proof. ∎

COROLLARY 3.5 (conservation). *The algorithm* $U^n \longrightarrow U_H^{n+1}$ *defined in* (3.13) *is conservative in the sense that* $\int_\Omega u_{h,H}^{n+1}\,d\boldsymbol{x} = \int_\Omega u_h^n\,d\boldsymbol{x}$.

Proof. Proceeding as in the proof of Proposition 3.3, we have

$$\int_\Omega (u_{h,H}^{n+1}-u_h^n)\,\mathrm{d}\boldsymbol{x} = \sum_{i=1}^N m_i(U_{H,i}^{n+1}-U_i^n) = -\Delta t\sum_{i=1}^N\left(G_i+\sum_{j=1}^N \mathcal{B}_{ij}G_j\right).$$

We conclude using Lemma 3.4 and the property $\sum_{i=1}^N G_i = 0$ which follows from the conservation property of b_K and the assumptions on the boundary conditions. ∎

3.4. Flux correction. We are now going to adapt the Boris–Book–Zalesak flux correction technique to u_H^{n+1} to ascertain that the solution at time t^{n+1} satisfies the local maximum principle. This theory is purely algebraic and is recalled in Appendix A for the reader's convenience; we also refer the reader to Kuzmin, Löhner, and Turek [23] for more details.

First we recast the definition of u_H^{n+1} in the form of (A.2). Denoting $F\in\mathbb{R}^N$ the column vector with entries

$$F_i := \sum_{K\subset S_i}\left(\nu_K^{L,n}b_K(u_h^n,\varphi_i)+\int_K \nabla\cdot(\boldsymbol{f}(u_h^n))\varphi_i\,\mathrm{d}\boldsymbol{x}\right), \tag{3.14}$$

the definition of $u_{h,L}^{n+1}$ gives $U_L^{n+1} = U^n - \Delta t^n(\mathcal{M}^L)^{-1}F$, which, together with the definition of $u_{h,H}^{n+1}$ (see (3.13)), in turn implies that

$$\begin{aligned}\mathcal{M}^L U_H^{n+1} &= \mathcal{M}^L U^n - \Delta t^n(\mathcal{I}+\mathcal{B})G = \mathcal{M}^L U^n - \Delta t^n F - \Delta t^n(G-F+\mathcal{B}G)\\ &= \mathcal{M}^L U_L^{n+1} - \Delta t^n(G-F+\mathcal{B}G).\end{aligned}$$

Using the conservation property of b_K, the difference $G-F$ can be rewritten as follows:

$$\begin{aligned}G_i-F_i &= \sum_{K\subset S_i}(\nu_K^{H,n}-\nu_K^{L,n})b_K(u_h^n,\varphi_i)\\ &= \sum_{i\neq j\in\mathcal{I}(S_i)}\sum_{K\subset S_i}(\nu_K^{H,n}-\nu_K^{L,n})U_j^n b_K(\varphi_j,\varphi_i)+\sum_{K\subset S_i}(\nu_K^{H,n}-\nu_K^{L,n})U_i^n b_K(\varphi_i,\varphi_i)\\ &= \sum_{i\neq j\in\mathcal{I}(S_i)}\sum_{K\subset S_i}(\nu_K^{H,n}-\nu_K^{L,n})(U_j^n-U_i^n)b_K(\varphi_j,\varphi_i).\end{aligned}$$

We then define the sparse matrix $\mathcal{A}^1\in\mathbb{R}^{N\times N}$ with entries

$$\mathcal{A}_{ij}^1 := \Delta t^n\sum_{K\subset S_i}(\nu_K^{L,n}-\nu_K^{H,n})(U_j^n-U_i^n)b_K(\varphi_j,\varphi_i). \tag{3.15}$$

Note that the sparsity pattern of $\mathcal{A}^1$ is the same as that of the consistent mass matrix; i.e., assembling $\mathcal{A}^1$ can be done the same way the mass matrix is assembled.

Using Lemma 3.4 (which implies that $\mathcal{B}_{ii} = -\sum_{i\neq j\in\mathcal{S}_i}\mathcal{B}_{ji}$) together with the property that the matrix $\mathcal{B}$ has the same sparsity pattern as the consistent mass matrix, we rewrite the product $\mathcal{B}G$ as follows:

$$(\mathcal{B}G)_i = \sum_{j\in\mathcal{S}_i}\mathcal{B}_{ij}G_j = \sum_{i\neq j\in\mathcal{S}_i}\mathcal{B}_{ij}G_j - \mathcal{B}_{ii}G_i = \sum_{i\neq j\in\mathcal{S}_i}(\mathcal{B}_{ij}G_j-\mathcal{B}_{ji}G_i). \tag{3.16}$$

We then define the second matrix $\mathcal{A}^2$ with entries

$$\mathcal{A}_{ij}^2 := -\Delta t^n(\mathcal{B}_{ij}G_j-\mathcal{B}_{ji}G_i). \tag{3.17}$$

Finally, setting $\mathcal{A} := \mathcal{A}^1 + \mathcal{A}^2$, the definition of U_H^{n+1} can be recast into the following form which is now suitable to apply the flux correction technique:

$$m_i U_{H,i}^{n+1} = m_i U_{L,i}^{n+1} + \sum_{j \in \mathcal{I}(S_i)} \mathcal{A}_{ij}. \tag{3.18}$$

Let $U_i^{\min} = \min_{j \in \mathcal{I}(i)} U_i^n$ and $U_i^{\max} = \max_{j \in \mathcal{I}(i)} U_i^n$, and denote $U^{\min} \in \mathbb{R}^N$ and $U^{\max} \in \mathbb{R}^N$ the two vectors whose entries are $U_i^{\min}$ and $U_i^{\max}$, $1 \le i \le N$. Note that Theorem 3.1 implies that

$$U_i^{\min} \le U_{L,i}^{n+1} \le U_i^{\max} \quad \forall i \in \{1, \dots, N\}. \tag{3.19}$$

The flux correction limiter is defined as follows. First, compute the coefficients P_i^+, P_i^-, Q_i^+, Q_i^-, R_i^+, and R_i^- $\forall 1 \le i \le N$:

$$P_i^+ := \sum_{j \in \mathcal{S}(i)} \max\{0, \mathcal{A}_{ij}\}, \qquad P_i^- := \sum_{j \in \mathcal{S}(i)} \min\{0, \mathcal{A}_{ij}\}. \tag{3.20}$$

$$Q_i^+ := m_i (U_i^{\max} - U_{L,i}^{n+1}), \quad Q_i^- := m_i (U_i^{\min} - U_{L,i}^{n+1}), \tag{3.21}$$

$$R_i^+ := \begin{cases} \min\{1, \frac{Q_i^+}{P_i^+}\} & \text{if } P_i^+ \neq 0, \\ 1 & \text{otherwise,} \end{cases} \quad R_i^- := \begin{cases} \min\{1, \frac{Q_i^-}{P_i^-}\} & \text{if } P_i^- \neq 0, \\ 1 & \text{otherwise.} \end{cases} \tag{3.22}$$

Then define the limiting coefficients $\mathcal{L}_{ij}$ $\forall 1 \le i, j \le N$ as follows:

$$\mathcal{L}_{ij} := \begin{cases} \min\{R_i^+, R_j^-\} & \text{if } \mathcal{A}_{ij} \ge 0, \\ \min\{R_i^-, R_j^+\} & \text{otherwise.} \end{cases} \tag{3.23}$$

Finally, the flux-corrected high-order solution at t^{n+1} is defined by

$$m_i U_i^{n+1} = m_i U_{L,i}^{n+1} + \sum_{j_\in \mathcal{I}(S_i)} \mathcal{L}_{ij} \mathcal{A}_{ij}. \tag{3.24}$$

In summary, given U^n, the algorithm $U^n \longrightarrow U^{n+1}$ consists of the following steps:

(i) Compute the first-order solution U_L^{n+1} defined in (3.5);
(ii) compute the entropy viscosity $\nu^{H,n}$ defined in (3.11);
(iii) compute the high-order right-hand side G defined in (3.12);
(iv) compute the matrices $\mathcal{A}^1$ and $\mathcal{A}^2$ defined in (3.15) and (3.17);
(v) compute the $\mathcal{L}$ matrix defined in (3.23);
(vi) update U^{n+1} by using (3.24).

We now formulate the main result of this section.

THEOREM 3.6 (discrete maximum principle). *In addition to the above assumptions, assume that* $\frac{\beta \Delta t^n}{h} \le \frac{1}{\lambda(1+\rho^{-1})}$. *Then the algorithm* $U^n \longrightarrow U^{n+1}$ *with* U^{n+1} *defined in* (3.24) *is conservative and satisfies the local discrete maximum principle, i.e.,* $u_{\min} \le \min_{j \in \mathcal{I}(S_i)} U_j^n \le U_i^{n+1} \le \max_{j \in \mathcal{I}(S_i)} U_j^n \le u_{\max}$ $\forall n \ge 0$.

Proof. We start by verifying that the assumptions of Lemma A.2 hold. The positivity condition (A.3) is satisfied by the assumption (2.3). The skew symmetry of $\mathcal{A}^1$ is a consequence of the symmetry of b_K (see definition of $\mathcal{A}^1$, (3.15)), and the skew symmetry of $\mathcal{A}^2$ is evident by construction (see (3.17)); as a result, $\mathcal{A}$ satisfies the skew symmetry assumption (A.4). The conservation properties (A.5) have been

established in Proposition 3.3 and Corollary 3.5. We can now apply Theorem 3.1 and Lemma A.2. ∎

COROLLARY 3.7 (maximum principle). *Under the assumptions of Theorem* 3.6, *the solution to the algorithm* $U^n \longrightarrow U^{n+1}$ *with* U^{n+1} *defined in* (3.24) *satisfies the following* L^∞*-estimates:*

$$c_{\min}u_{\min} \le u_h^n(\boldsymbol{x}) \le c_{\max}u_{\max} \quad \forall n \ge 0,\ \forall \boldsymbol{x} \in \Omega. \tag{3.25}$$

Moreover, if the space X_h *is such that* $\min_{\ell\in\mathcal{I}(K)} v(\boldsymbol{a}_\ell) \le v(\boldsymbol{x}) \le \max_{\ell\in\mathcal{I}(K)} v(\boldsymbol{a}_\ell)$ $\forall v \in X_h$, $\forall \boldsymbol{x} \in K$, $\forall K \in \mathcal{K}_h$, *then the following holds for all* $K \in \mathcal{K}_h$*:*

$$\min_{i\in\mathcal{I}(K)} \min_{j\in\mathcal{I}(S_i)} U_j^n \le u_h^{n+1}(\boldsymbol{x}) \le \max_{i\in\mathcal{I}(K)} \max_{j\in\mathcal{I}(S_i)} U_j^n \quad \forall n \ge 0. \tag{3.26}$$

Remark 3.2. Note that (3.26) holds for $\mathbb{P}_1$ and $\mathbb{Q}_1$ finite elements, but only (3.25) can be guaranteed for higher-order elements. Preliminary numerical results (not reported here) using $\mathbb{Q}_2$, $\mathbb{Q}_3$, and $\mathbb{P}_3$ finite elements confirm the results of Corollary 3.7. In these tests, the coefficient λ defined in (2.4) is no longer equal to 1 and grows with the polynomial degree, which in turns decreases the admissible CFL. A possible way to overcome this obstacle is under investigation and will be reported in due time.

4. Numerical illustrations. In this section we present numerical illustrations of the algorithm introduced above (see (3.24)). Henceforth, the "limiter solution" is the result of (3.24), and the "entropy viscosity solution" is the result of (3.24) with no limiter, i.e., $\mathcal{L}_{ij} = 1$. All the computations are done in two space dimensions using continuous $\mathbb{P}_1$ finite elements for the space approximation and SSP RK3 to step in time (see Gottlieb, Shu, and Tadmor [11]). The implementation is done with the open source finite element library DOLFIN; see Logg and Wells [26]. We first solve in section 4.1 a linear transport problem with smooth data to assess the accuracy of the method; then we test the method on bounded variation initial data. In section 4.2, we test the convergence properties of the algorithm by solving two nonlinear scalar conservation equations.

4.1. Linear transport problem. Let us consider the two-dimensional rotation field $\boldsymbol{\beta}(\boldsymbol{x}) = 2\pi(-x_2, x_1)$ and the linear transport equation:

$$\partial_t u(\boldsymbol{x},t) + \boldsymbol{\beta}(\boldsymbol{x})\cdot\nabla u(\boldsymbol{x},t) = 0, \quad u(\boldsymbol{x},0) = u_0(\boldsymbol{x}). \tag{4.1}$$

In all the tests reported in this section the entropy viscosity is computed with $c_E = 1$ and $c_J = 1$, and the entropy residual is computed with the entropy $E(u) = -\ln(|u(1-u)| + \epsilon)$ with $\epsilon = 10^{-10}$. The CFL number is set to 0.3.

4.1.1. Smooth solution. We solve (4.1) up to $t = 1$ in $\mathbb{R}^2$ with the following smooth initial data:

$$u_0(\boldsymbol{x}) = \tfrac{1}{2}\left(1 - \tanh\left(\tfrac{(\boldsymbol{x}-\boldsymbol{x}_0)^2}{r_0^2} - 1\right)\right), \quad \text{with} \quad r_0 = 0.25,\ \boldsymbol{x}_0 = (0.3, 0). \tag{4.2}$$

Two types of meshes are tested. First, the computational domain is restricted to the unit disc, and we use unstructured triangular meshes in this domain. Second, the computational domain is restricted to the unit square, $[-1,1]^2$, and we use structured triangular meshes therein. The structured meshes are obtained by dividing the unit square into small rectangles and by cutting each small rectangle in half from the top left corner to the bottom right corner. For each of the above two mesh configurations,

TABLE 1

Smooth data, unstructured $\mathbb{P}_1$ meshes, and convergence tests for entropy viscosity and limiter solution.

h	$\mathbb{P}_1$ entropy viscosity					
	L^1	rate	L^2	rate	L^∞	rate
0.1	9.78E-02	–	1.09E-01	–	2.65E-01	–
0.05	2.52E-02	2.02	3.09E-02	1.88	9.41E-02	1.54
0.025	4.33E-03	2.65	5.64E-03	2.56	1.91E-02	2.41
0.0125	7.38E-04	2.56	9.26E-04	2.61	5.48E-03	1.80
0.00625	1.52E-04	2.28	1.99E-04	2.22	2.38E-03	1.20
h	$\mathbb{P}_1$ limiter solution					
	L^1	rate	L^2	rate	L^∞	rate
0.1	9.40E-02	–	1.05E-01	–	2.58E-01	–
0.05	2.40E-02	2.04	2.92E-02	1.91	8.68E-02	1.63
0.025	4.48E-03	2.53	5.84E-03	2.43	2.02E-02	2.20
0.0125	8.15E-04	2.46	1.02E-03	2.53	5.28E-03	1.94
0.00625	1.75E-04	2.22	2.31E-04	2.14	2.40E-03	1.13

TABLE 2

Smooth data, uniform $\mathbb{P}_1$ meshes, and convergence tests for entropy viscosity and limiter solution.

h	$\mathbb{P}_1$ entropy viscosity					
	L^1	rate	L^2	rate	L^∞	rate
0.1	1.36E-01	–	1.48E-01	–	3.64E-01	–
0.05	3.91E-02	1.87	4.86E-02	1.67	1.28E-01	1.56
0.025	7.64E-03	2.40	1.09E-02	2.20	3.24E-02	2.02
0.0125	1.16E-03	2.74	1.73E-03	2.68	5.42E-03	2.60
0.00625	1.70E-04	2.78	2.50E-04	2.81	7.79E-04	2.81
h	$\mathbb{P}_1$ limiter solution					
	L^1	rate	L^2	rate	L^∞	rate
0.1	1.32E-01	–	1.45E-01	–	3.64E-01	–
0.05	3.62E-02	1.93	4.47E-02	1.75	1.17E-01	1.70
0.025	7.58E-03	2.30	1.09E-02	2.08	3.25E-02	1.87
0.0125	1.16E-03	2.73	1.74E-03	2.66	5.44E-03	2.60
0.00625	1.72E-04	2.77	2.53E-04	2.80	1.41E-03	1.96

we test five meshsizes $h = 0.1$, 0.05, 0.025, 0.0125, and 0.00625. The L^1-, L^2-, and L^∞-norms of the error are evaluated at time $t = 1$, i.e., after one revolution. The results for the unstructured meshes are shown in Table 1, and those for the structured meshes are shown in Table 2.

The results from both the uniform and unstructured meshes indicate that the entropy viscosity solution and the limiter solution achieve optimal convergence rates in the L^1- and L^2-norms. The diagnostic in the L^∞-norm is less clear; when compared to the entropy solution it seems that the limiter solution on structured grids suffers from a slight optimality loss in the L^∞-norm. On the other hand, the errors in all norms for the entropy viscosity solution and the limiter solution on unstructured grids are almost identical; i.e., the effect of the limiter is unnoticeable.

Finally, we evaluate the effect of the mass lumping correction done in (3.13) by performing two computations up to $t = 4$ (four revolutions) on an unstructured mesh composed of 6773 $\mathbb{P}_1$ nodes. One computation is done with the mass lumping correction (see the middle panel in Figure 1), and the other is done without (see the right panel in Figure 1). The dispersion effects of mass lumping and the correction thereof are clearly visible. This test confirms the validity of our mass lumping correction approach.

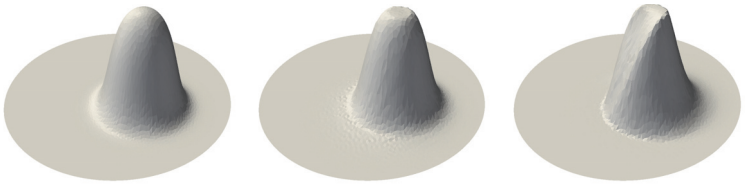

FIG. 1. *Rotation of smooth data, unstructured mesh,* 6773 $\mathbb{P}_1$ *nodes,* $t = 4$. *Exact solution (left), limiter solution with lumped mass matrix correction (center), and limiter solution with lumped mass matrix (right).*

4.1.2. Three body rotation. The method is now evaluated on the transport problem (4.1) with the following nonsmooth initial data which is commonly used in the literature:

$$u_0(\boldsymbol{x}) = \begin{cases} 1 & \text{if } \|\boldsymbol{x}-\boldsymbol{x}_d\| \le r_0 \text{ and } (|x_1| \ge 0.05 \text{ or } x_2 \ge 0.7), \\ 1 - \frac{\|\boldsymbol{x}-\boldsymbol{x}_c\|}{r_0} & \text{if } \|\boldsymbol{x}-\boldsymbol{x}_c\| \le r_0, \\ g(\|\boldsymbol{x}-\boldsymbol{x}_h\|) & \text{if } \|\boldsymbol{x}-\boldsymbol{x}_h\| \le r_0, \\ 0 & \text{otherwise,} \end{cases} \tag{4.3}$$

where $r_0 = 0.3$, $g(r) := \frac{1}{4}[1 + \cos(\pi \min(\frac{r}{r_0}, 1))]$, $\boldsymbol{x}_d = (0, 0.5)$, $\boldsymbol{x}_c = (0, -0.5)$, and $\boldsymbol{x}_h = (-0.5, 0)$. The graph of u_0 consists of three bodies: a slotted cylinder of height 1, a smooth hump of height $\frac{1}{2}$, and a cone of height 1 (see leftmost panel in Figure 3). Two series of tests are performed: one is done on structured meshes in the domain $[-1, 1]^2$; the other is done on unstructured triangular meshes; $\mathbb{P}_1$ elements are used in both cases.

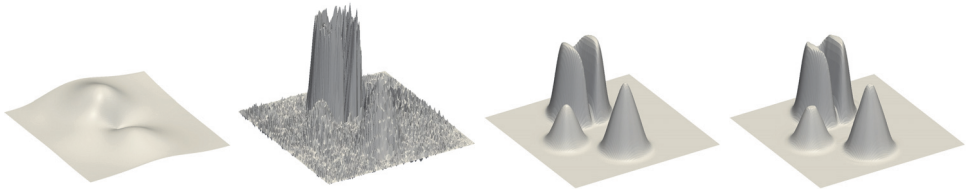

FIG. 2. *Uniform mesh,* 128×128, $t = 1$*: First-order viscosity solution (left); Galerkin* $-0.422 \le u \le 1.36$ *(center left); entropy viscosity solution* $-3.2\times10^{-8} \le u \le 0.978$ *(center right); limiter solution* $0 \le u \le 0.965$ *(right).*

We first compare the performance of the algorithm presented in this paper with that of the first-order viscosity method, the Galerkin method (i.e., no stabilization), and the entropy viscosity method (i.e., no limiter). This test is done on the square $[-1, 1]^2$ using a uniform mesh composed of 128×128 $\mathbb{P}_1$ nodes. The first-order solution, the Galerkin solution, the entropy viscosity solution, and the limiter solution at $t = 1$ are shown in Figure 2 from left to right. The first-order solution satisfies the maximum principle but is clearly inaccurate. The Galerkin solution suffers from spurious oscillations. The Galerkin solution is improved significantly by augmenting it with the entropy viscosity; however, the local maximum principle is slightly violated. The limiter corrects the small maximum principle violations of the entropy viscosity method, as proven in the above theory.

We show in Table 3 convergence tests performed on five successively refined uniform meshes of the square $[-1, 1]^2$. The convergence rates in the L^1- and L^2-norms

TABLE 3
Three body rotation, convergence tests, uniform $\mathbb{P}_1$ meshes: Entropy viscosity and limiter solution.

h	$\mathbb{P}_1$ entropy viscosity				$\mathbb{P}_1$ limiter solution			
	L^1	rate	L^2	rate	L^1	rate	L^2	rate
0.1	3.94E-01	–	3.47E-01	–	4.05E-01	–	3.55E-01	–
0.05	2.37E-01	0.76	2.54E-01	0.47	2.42E-01	0.77	2.57E-01	0.48
0.025	1.34E-01	0.84	1.96E-01	0.38	1.37E-01	0.84	2.00E-01	0.37
0.0125	8.10E-02	0.74	1.48E-01	0.41	8.22E-02	0.74	1.49E-01	0.43
0.00625	4.89E-02	0.73	1.14E-01	0.38	4.93E-02	0.74	1.14E-01	0.39

are approximately 0.74 and 0.37, respectively; these rates are consistent with those reported in Guermond, Pasquetti, and Popov [17, Table 3.4]. The best possible theoretical approximation rates on these types of meshes are 1 and 0.5, respectively. Note again that the limiter does not degrade the accuracy of the entropy viscosity solution.

We now perform convergence tests on nonuniform meshes in the unit disc $\{\boldsymbol{x} \in \mathbb{R}^2 \mid \|\boldsymbol{x}\| \leq 1\}$. We use $\mathbb{P}_1$ finite elements on five successively refined meshes: $h = 0.1$, 0.05, 0.025, 0.0125, and 0.00625. The graph of the limiter solution at $t = 1$ on each of these meshes is shown in Figure 3. Again the algorithm converges without showing distortions due to dispersion error. We have numerically verified that the local maximum principle is indeed satisfied at each time step, as claimed in Theorem 3.6 (actually the verification is done at each SSP RK3 subtstep).

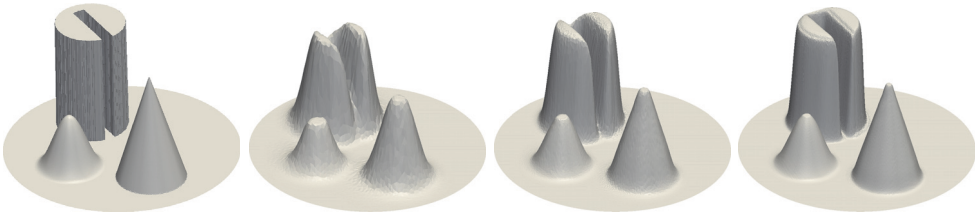

FIG. 3. *Limiter solution on unstructured meshes, $t = 1$: 1789 nodes, $0.1\times10^{-6} \leq u \leq 0.69$ (left); 6773 nodes, $0 \leq u \leq 0.89$ (center left); 26969 nodes, $0 \leq u \leq 0.989$ (center right); 107696 nodes, $0 \leq u \leq 1$ (right).*

Table 4 presents the results for the above convergence tests on the unstructured grids. The convergence rates are quite similar to what is observed on the structured grids (see Table 3); i.e., the convergence rates in the L^1- and L^2-norms are $0.73 \sim 0.76$ and $0.37 \sim 0.38$, respectively. Note again that the limiter does not degrade the accuracy of the entropy viscosity solution.

TABLE 4
Three body rotation, convergence tests, unstructured meshes: Entropy viscosity versus limiter solution.

h	$\mathbb{P}_1$ entropy viscosity				$\mathbb{P}_1$ limiter solution			
	L^1	rate	L^2	rate	L^1	rate	L^2	rate
0.1	3.57E-01	–	3.35E-01	–	3.60E-01	–	3.36E-01	–
0.05	2.12E-01	0.77	2.48E-01	0.44	2.19E-01	0.74	2.57E-01	0.40
0.025	1.22E-01	0.84	1.82E-01	0.46	1.25E-01	0.85	1.85E-01	0.49
0.0125	6.97E-02	0.81	1.34E-01	0.44	7.11E-02	0.81	1.35E-01	0.46
0.00625	4.11E-02	0.76	1.03E-01	0.38	4.19E-02	0.76	1.03E-01	0.39

4.1.3. Conclusions. The above convergence tests confirm that the proposed method is (at least) fully second-order and performs equally well on structured and unstructured grids. The tests also confirm that the mass lumping correction as defined in (3.13) is an important ingredient of the method (see Figure 1).

4.2. Nonlinear problems. In this section the method is tested for convergence towards the entropy solution on two nonlinear scalar conservation equations. The entropy used to compute the entropy residual for this problem is $E(u) = \frac{1}{2}u^2$, and the entropy viscosity is computed with $c_E = 1$, $c_J = 4$. All the computations are done with CFL = 0.3.

4.2.1. Burgers' equation. Consider the two-dimensional Burgers' equation:

$$\partial_t u + \nabla\cdot\left(\tfrac{1}{2}\boldsymbol{\beta}u^2\right) = 0, \qquad u(\boldsymbol{x},0) = u_0(\boldsymbol{x}), \tag{4.4}$$

where $\boldsymbol{\beta} = (1,1)$ and the initial condition u_0 is given by

$$u_0 = \begin{cases} -0.2 & \text{if } x_1 < 0.5 \text{ and } x_2 > 0.5, \\ -1 & \text{if } x_1 > 0.5 \text{ and } x_2 > 0.5, \\ 0.5 & \text{if } x_1 < 0.5 \text{ and } x_2 < 0.5, \\ 0.8 & \text{if } x_1 > 0.5 \text{ and } x_2 < 0.5. \end{cases} \tag{4.5}$$

The exact solution to this problem is available in Guermond, Pasquetti, and Popov [17, eq. (4.3)]. The problem is solved in the square $[0,1]^2$ up to $t = 0.5$, and the computational domain is triangulated using six successively refined unstructured meshes: $h = 0.1, 0.05, \ldots, 0.003125$.

Table 5 shows the convergence results for both the entropy viscosity solution and the limiter solution. Observe that the convergence rates in the L^1- and L^2-norms are close to the optimal rates, i.e., almost 1 and $\frac{1}{2}$, respectively.

TABLE 5
Burgers' equation, convergence tests, unstructured meshes: Entropy viscosity versus limiter solution.

h	$\mathbb{P}_1$ entropy viscosity				$\mathbb{P}_1$ limiter solution			
	L^1	rate	L^2	rate	L^1	rate	L^2	rate
0.1	1.06E-01	–	2.32E-01	–	8.49E-02	–	1.98E-01	–
0.05	5.68E-02	0.90	1.64E-01	0.50	3.73E-02	1.20	1.28E-01	0.64
0.025	2.92E-02	0.98	1.21E-01	0.44	2.10E-02	0.85	9.77E-02	0.39
0.0125	1.60E-02	0.89	9.39E-02	0.38	1.17E-02	0.86	7.72E-02	0.35
0.00625	7.91E-03	1.00	6.64E-02	0.50	5.64E-03	1.10	5.52E-02	0.49
0.003125	4.06E-03	0.97	4.85E-02	0.45	2.90E-03	0.96	4.04E-02	0.45

To have a better appreciation of the amount of maximum principle violation by the entropy viscosity solution and visualize the action of the flux correction technique, we show in Figure 4 a cross section along the line $x_2 = 1 - x_1$ of the graph of the entropy viscosity and limiter solutions at $t = 0.5$ on four different meshes. The cross section for the entropy solution is shown in the left panel, and that for the limiter solution is shown in the right panel. Two regions are magnified to emphasize the slight violations of the local maximum principle by the entropy viscosity solution. Using the curvilinear abscissa $s = \sqrt{2}x_1$, the first region is the rectangle $(s,u) \in [1.35 \pm 0.075]\times[0.8 \pm 7.5\times10^{-4}]$; the second region is $(s,u) \in [0.55 \pm 0.3]\times[-1 \pm 7.5\times10^{-4}]$. Observe that in both cases the over- and undershoots of the entropy solution are barely noticeable and seem to diminish as the meshes are refined. Note also that the

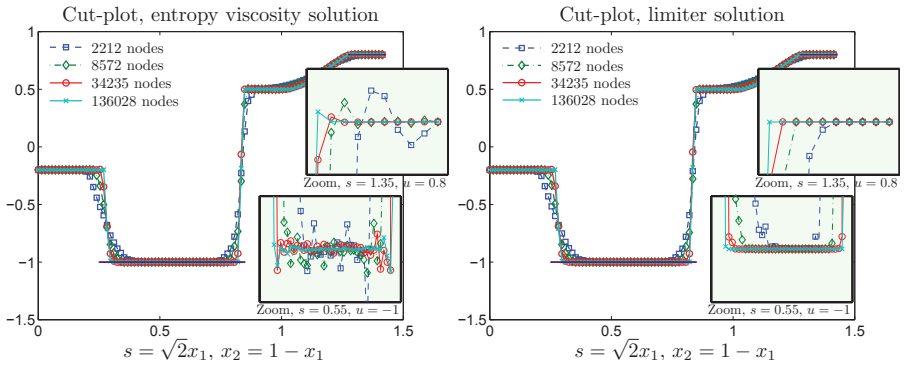

FIG. 4. *Cross section: Burgers' equation.*

limiter solution definitely satisfies the maximum principle, and the convergence of the limiter solution to the exact solution seems to be monotone.

4.2.2. KPP rotating wave. In this section we solve a two-dimensional scalar conservation equation with a nonconvex flux:

$$\partial_t u + \nabla \cdot \boldsymbol{f}(u) = 0, \quad u(\boldsymbol{x}, 0) = u_0(\boldsymbol{x}) = \begin{cases} \frac{14\pi}{4} & \text{if } \sqrt{x^2 + y^2} \le 1, \\ \frac{\pi}{4} & \text{otherwise,} \end{cases} \tag{4.6}$$

where $\boldsymbol{f}(u) = (\sin u, \cos u)$. This test was originally proposed in Kurganov, Petrova, and Popov [21]. It is a challenging test case for many high-order numerical schemes because the solution has a two-dimensional composite wave structure. For example, it has been shown in [21] that some central-upwind schemes based on WENO5, Minmod 2, and SuperBee reconstructions converge to nonentropic solutions.

The computational domain $[-2, 2]\times[-2.5, 1.5]$ is triangulated using nonuniform meshes, and the solution is approximated up to $t = 1$ using $\mathbb{P}_1$ finite elements. The graph of the limiter solution on four meshes (2208, 8560, 34268, and 135841 $\mathbb{P}_1$ nodes, respectively) is shown in Figure 5. The helicoidal composite wave is clearly visible.

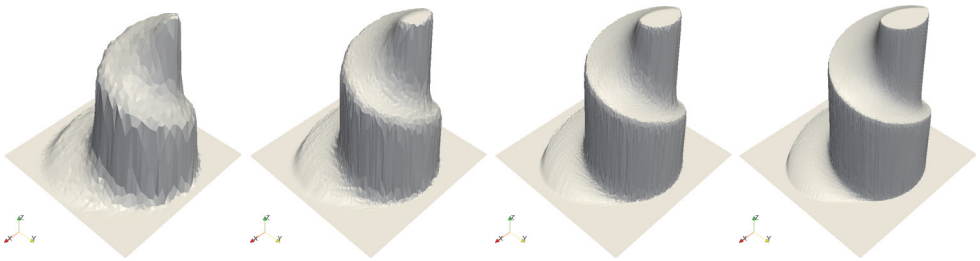

FIG. 5. *Limiter solution on unstructured meshes:* 2208 *nodes (left);* 8560 *nodes (center left);* 34268 *nodes (center right);* 135841 *nodes (right).*

To better evaluate the amount of maximum principle violation by the entropy viscosity solution and visualize the action of the flux correction technique, we show in Figure 6 a cross section along the line $x_2 = x_1$ of the graph of the entropy viscosity and limiter solutions at $t = 1$ on four different meshes (2208, 8560, 34268, and 135841 $\mathbb{P}_1$ nodes, respectively). The cross section for the entropy solution is shown in the

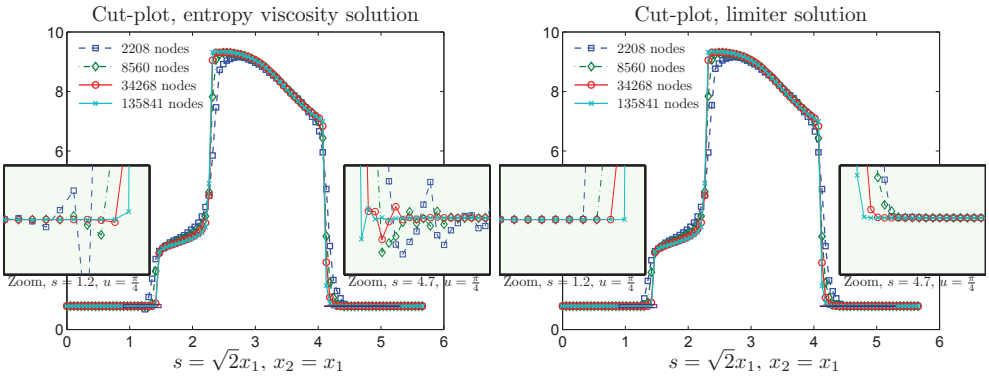

FIG. 6. *Cross section: KPP problem.*

left panel and that for the limiter solution is shown in the right panel. Two regions are magnified to emphasize the slight violations of the local maximum principle by the entropy viscosity solution. Using the curvilinear abscissa $s = \sqrt{2}x_1$, the first region is the rectangle $(s,u) \in [1.2 \pm 0.3]\times[\frac{\pi}{4} \pm 5\times10^{-2}]$, and the second region is the rectangle $(s,u) \in [4.7 \pm 0.6]\times[\frac{\pi}{4} \pm 1\times10^{-2}]$. Observe that in both cases the over- and undershoots of the entropy solution are barely noticeable and seem to diminish as the meshes are refined. Note again that the limiter solution satisfies the maximum principle, and the convergence of the limiter solution to the exact solution seems to be monotone.

4.2.3. Convergence to the entropy solution. It may be tempting to think that limiting can be used directly on the Galerkin solution, i.e., using $\nu^{H,n} = 0$ in (3.12). This intuition is wrong since there is no mechanism in the limiter to add the correct entropy-satisfying dissipation. To illustrate this phenomenon, we solve the Kurganov–Petrova–Popov (KPP) problem on the three unstructured grids used in the previous section (see Figure 5) using (3.24) with $\nu^{H,n} = 0$. The results are shown in Figure 7.

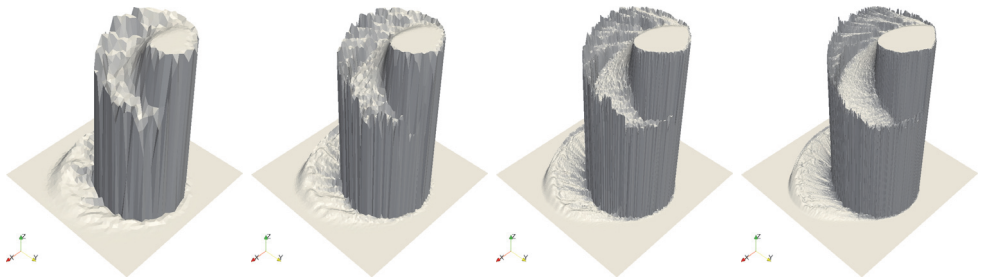

FIG. 7. *KPP problem, Galerkin solution + limiter on unstructured meshes:* 2208 *nodes (left);* 8560 *(center left);* 34268 *nodes (center right);* 135841 *nodes (right).*

Although the solution satisfies the local maximum principle at every grid point and at every SSP RK3 substep, the approximate solution seems to converge to a weak solution which is not the unique entropy solution. This observation is in agreement with the experiments from Kurganov, Petrova, and Popov [21]. This observation also shows that the high-order method in (3.24) must have the correct entropy dissipation

for the present technique to converge properly. This justifies the entropy-viscosity strategy that we have adopted. Note finally that this example illustrates well that satisfying the local maximum principle does not imply total variation diminution.

4.2.4. Conclusions. In conclusion, the new limited entropy-viscosity method presented in this paper is (i) higher-order accurate (at least second-order); (ii) maximum principle preserving; and (iii) convergent. Items (i) and (iii) are numerical observations, and item (ii) is proved in Theorem 3.6 and Corollary 3.7. Note finally that the modifications done by the limiter on the entropy viscosity solution are barely noticeable in general. In the words of Babuška, it could be said that the limiter is the validation stamp on the method certifying that it is maximum principle satisfying. Note finally that while a proof that the whole algorithm converges to the entropy solution is still missing, the first-order method does converge as described (Guermond, Nazarov, and Popov [14]).

Appendix A. The Boris–Book–Zalesak theory. For the reader's convenience, we recall in this section the main feature of the limiter theory developed by Boris and Book [3] and Zalesak [33]; we refer the reader to Kuzmin and Turek [24] for a comprehensive review.

This theory is essentially algebraic. Let $U^n \in \mathbb{R}^N$ and assume that we have two Markov processes $U^n \to U_L^{n+1}$ and $U^n \to U_H^{n+1}$ where we refer to U_L^{n+1} and U_H^{n+1} as the low- and high-order solutions, respectively. We assume that the low-order solution satisfies some minimum and maximum principle; say there are two vectors $U^{\min} \in \mathbb{R}^N$ and $U^{\max} \in \mathbb{R}^N$ such that

$$U_i^{\min} \le U_{L,i}^{n+1} \le U_i^{\max} \quad \forall i \in \{1, \dots, N\}. \tag{A.1}$$

For instance, $U_i^{\min} = \min_{j\in\mathcal{I}(i)} U_i^n$ and $U_i^{\max} = \max_{j\in\mathcal{I}(i)} U_i^n$ are possible definitions of $U^{\min}$ and $U^{\max}$, where $\mathcal{I}(i)$ is a set of indices that depends on i (think of the indices of the shape functions φ_j whose support has nonzero intersection with the shape function φ_i). We assume also that $j \in \mathcal{I}(i)$ if and only $i \in \mathcal{I}(j)$. We furthermore assume that U_L^{n+1} and U_H^{n+1} are related as follows:

$$m_i U_{H,i}^{n+1} = m_i U_{L,i}^{n+1} + \sum_{j\in\mathcal{I}(i)} a_{ij}, \tag{A.2}$$

where the coefficients m_i and a_{ij} satisfy the following properties:

$$m_i > 0, \qquad 1 \le i \le N, \tag{A.3}$$

$$a_{ij} = -a_{ji}, \qquad 1 \le i, j \le N. \tag{A.4}$$

We finally assume that the two processes $U^n \to U_L^{n+1}$ and $U^n \to U_H^{n+1}$ satisfy the following additional conservation property:

$$\sum_i m_i U_{L,i}^{n+1} = \sum_i m_i U_i^n, \qquad \sum_i m_i U_{H,i}^{n+1} = \sum_i m_i U_i^n \qquad \forall n \ge 0, \tag{A.5}$$

and we refer to the above identities by saying that the processes $U^n \to U_L^{n+1}$ and $U^n \to U_H^{n+1}$ are conservative.

Since it is not guaranteed that U_H^{n+1} satisfies the minimum and maximum principle, Boris and Book [3], Zalesak [33], and Kuzmin and Turek [24] propose to modify

the high-order solution as follows:

$$m_i U_i^{n+1} = m_i U_{L,i}^{n+1} + \sum_{j\in\mathcal{I}(i)} \mathcal{L}_{ij} a_{ij}, \tag{A.6}$$

where the limiting coefficients $\mathcal{L}_{ij}$ are computed using the following procedure. First, compute the coefficients P_i^+, P_i^-, Q_i^+, Q_i^-, R_i^+, and R_i^-, $1 \le i \le N$:

$$P_i^+ := \sum_{j\in\mathcal{S}(i)} \max\{0, a_{ij}\}, \qquad P_i^- := \sum_{j\in\mathcal{S}(i)} \min\{0, a_{ij}\}, \tag{A.7}$$

$$Q_i^+ := m_i(U_i^{\max} - U_{L,i}^{n+1}), \qquad Q_i^- := m_i(U_i^{\min} - U_{L,i}^{n+1}), \tag{A.8}$$

$$R_i^+ := \begin{cases} \min\{1, \frac{Q_i^+}{P_i^+}\} & \text{if } P_i^+ \neq 0, \\ 1 & \text{otherwise,} \end{cases} \qquad R_i^- := \begin{cases} \min\{1, \frac{Q_i^-}{P_i^-}\} & \text{if } P_i^- \neq 0, \\ 1 & \text{otherwise.} \end{cases} \tag{A.9}$$

Then define the limiting coefficients $\mathcal{L}_{ij}$ that are used in (A.6) as follows:

$$\mathcal{L}_{ij} := \begin{cases} \min\{R_i^+, R_j^-\} & \text{if } a_{ij} \ge 0, \\ \min\{R_i^-, R_j^+\} & \text{otherwise.} \end{cases} \tag{A.10}$$

LEMMA A.1. *The definitions* (A.7), (A.8), (A.9), (A.10) *imply the following properties:*

$$P_i^- \le 0 \le P_i^+, \quad Q_i^- \le 0 \le Q_i^+, \quad 0 \le R_i^-, \quad 0 \le R_i^+ \qquad \forall i \in \{0, \dots, N\}, \tag{A.11}$$

$$0 \le \mathcal{L}_{ij} \le 1, \quad \mathcal{L}_{ij} = \mathcal{L}_{ji} \qquad \forall i, j \in \{0, \dots, N\}. \tag{A.12}$$

Proof. The properties (A.11) follow immediately from the definitions (A.7), (A.8), (A.9) and the assumption (A.1). The definitions of R_i^+ and R_j^- imply that $0 \le \mathcal{L}_{ij} \le 1$. Let us now prove that $\mathcal{L}_{ij} = \mathcal{L}_{ji}$. Assume that $a_{ij} \ge 0$. Then $a_{ji} = -a_{ij} \le 0$ owing to (A.4). The definition of $\mathcal{L}_{ij}$ and $\mathcal{L}_{ji}$ imply in turn that $\mathcal{L}_{ij} = \min\{R_i^+, R_j^-\}$ and $\mathcal{L}_{ji} = \min\{R_j^-, R_i^+\}$; i.e., $\mathcal{L}_{ij} = \mathcal{L}_{ji}$. The proof for the case $a_{ij} \le 0$ is identical. ∎

The key property of the above limiting procedure is that it is conservative and gives a local maximum principle.

LEMMA A.2. *Let* $U^{\min} \in \mathbb{R}^N$ *and* $U^{\max} \in \mathbb{R}^N$ *be such that* (A.1) *holds. Under the above assumptions* (A.3), (A.4), (A.5), *the solution of the scheme* (A.6) *with* $\mathcal{L}_{ij}$ *defined as in* (A.10) *is conservative and satisfies*

$$U_i^{\min} \le U_i^{n+1} \le U_i^{\max}, \qquad i = 1, \dots, N. \tag{A.13}$$

Proof. (1) We first prove conservation. It suffices to show that $\sum_{i=1}^N m_i(U_i^{n+1} - U_{L,i}^{n+1}) = 0$ to conclude that $\sum_{i=1}^N m_i(U_i^{n+1} - U_i^n) = 0$. The symmetry properties of $\mathcal{L}_{ij}$ and a_{ij} imply that

$$\begin{aligned} \sum_{i=1}^N m_i\Big(U_i^{n+1} - U_{L,i}^{n+1}\Big) &= \sum_{i=1}^N \sum_{j\in\mathcal{I}(i)} \mathcal{L}_{ij} a_{ij} = \sum_{i\in\mathcal{I}(j), j\in\mathcal{I}(i)} (\mathcal{L}_{ij} a_{ij} + \mathcal{L}_{ji} a_{ji}) \\ &= \sum_{i\in\mathcal{I}(j), j\in\mathcal{I}(i)} (\mathcal{L}_{ij} a_{ij} - \mathcal{L}_{ij} a_{ij}) = 0. \end{aligned}$$

The conclusion follows readily.

(2) We now prove the local maximum principle, i.e., (A.13). Let us assume that $P_i^+ \neq 0$. By (A.6) and the definition of $\mathcal{L}_{ij}$, we have

$$\begin{aligned} m_i(U_i^{n+1} - U_{L,i}^{n+1}) :&= \sum_{j\in\mathcal{I}(i)} \mathcal{L}_{ij}a_{ij} \leq \sum_{j\in\mathcal{I}(i),\ 0\leq a_{ij}} \mathcal{L}_{ij}a_{ij} = \sum_{j\in\mathcal{I}(i),\ 0\leq a_{ij}} \min\{R_i^+, R_j^-\}a_{ij} \\ &\leq \sum_{j\in\mathcal{I}(i),\ 0\leq a_{ij}} R_i^+ a_{ij} \leq \sum_{j\in\mathcal{I}(i),\ 0\leq a_{ij}} \frac{Q_i^+}{P_i^+}a_{ij} \\ &= \frac{Q_i^+}{P_i^+} \sum_{j\in\mathcal{I}(i)} \max\{0, a_{ij}\} = Q_i^+ = m_i(U_i^{\max} - U_{L,i}^{n+1}), \end{aligned}$$

which proves that $U_i^{n+1} \leq U_i^{\max}$ when $P_i^+ \neq 0$. If $P_i^+ = 0$, then $m_i(U_i^{n+1} - U_{L,i}^{n+1}) \leq 0 \leq m_i(U_i^{\max} - U_{L,i}^{n+1})$, which proves again that $U_i^{n+1} \leq U_i^{\max}$. The lower bound, $U_i^{\min} \leq U_i^{n+1}$, is proved similarly. ∎

Remark A.1. Note that the above maximum principle holds independently of the definition of $U_i^{\max}$ and $U_i^{\min}$ provided that (A.1) holds.

Remark A.2. By Lemma A.2, it follows that if the low-order scheme satisfies the maximum principle, (A.1), then the maximum principle also holds for the new scheme (A.6).

REFERENCES

[1] S. Badia and A. Hierro, *On monotonicity-preserving stabilized finite element approximation of the transport problems*, SIAM J. Sci. Comput., submitted.

[2] C. Bardos, A. Y. le Roux, and J.-C. Nédélec, *First order quasilinear equations with boundary conditions*, Comm. Partial Differential Equations, 4 (1979), pp. 1017–1034.

[3] J. P. Boris and D. L. Book, *Flux-corrected transport. I. SHASTA, a fluid transport algorithm that works [J. Comput. Phys., 11 (1973), pp. 38–69]*, J. Comput. Phys., 135 (1997), pp. 170–186.

[4] E. Burman, *On nonlinear artificial viscosity, discrete maximum principle and hyperbolic conservation laws*, BIT, 47 (2007), pp. 715–733.

[5] E. Burman and A. Ern, *Nonlinear diffusion and discrete maximum principle for stabilized Galerkin approximations of the convection–diffusion-reaction equation*, Comput. Methods Appl. Mech. Engrg., 191 (2002), pp. 3833–3855.

[6] E. Burman and A. Ern, *Stabilized Galerkin approximation of convection-diffusion-reaction equations: Discrete maximum principle and convergence*, Math. Comp., 74 (2005), pp. 1637–1652.

[7] J. C. Campbell and M. J. Shashkov, *A tensor artificial viscosity using a mimetic finite difference algorithm*, J. Comput. Phys., 172 (2001), pp. 739–765.

[8] M. A. Christon, *The influence of the mass matrix on the dispersive nature of the semi-discrete, second-order wave equation*, Comput. Methods Appl. Mech. Engrg., 173 (1999), pp. 147–166.

[9] M. A. Christon, M. J. Martinez, and T. E. Voth, *Generalized Fourier analyses of the advection-diffusion equation—part I: One-dimensional domains*, Internat. J. Numer. Methods Fluids, 45 (2004), pp. 839–887.

[10] V. A. Dobrev, T. V. Kolev, and R. N. Rieben, *High-order curvilinear finite element methods for Lagrangian hydrodynamics*, SIAM J. Sci. Comput., 34 (2012), pp. B606–B641.

[11] S. Gottlieb, C.-W. Shu, and E. Tadmor, *Strong stability-preserving high-order time discretization methods*, SIAM Rev., 43 (2001), pp. 89–112.

[12] P. M. Gresho, R. L. Sani, and M. S. Engelman, *Incompressible Flow and the Finite Element Method: Advection-Diffusion and Isothermal Laminar Flow*, Wiley, New York, 1998.

[13] J.-L. Guermond and M. Nazarov, *A maximum-principle preserving C^0 finite element method for scalar conservation equations*, Comput. Methods Appl. Mech. Engrg., 272 (2014), pp. 198–213.

[14] J.-L. Guermond, M. Nazarov, and B. Popov, *Error Estimates for a First-Order Lagrange Finite Element Technique for Nonlinear Scalar Conservation Equations*, submitted.
[15] J.-L. Guermond and R. Pasquetti, *Entropy-based nonlinear viscosity for Fourier approximations of conservation laws*, C. R. Math. Acad. Sci. Paris, 346 (2008), pp. 801–806.
[16] J.-L. Guermond and R. Pasquetti, *A correction technique for the dispersive effects of mass lumping for transport problems*, Comput. Methods Appl. Mech. Engrg., 253 (2013), pp. 186–198.
[17] J.-L. Guermond, R. Pasquetti, and B. Popov, *Entropy viscosity method for nonlinear conservation laws*, J. Comput. Phys., 230 (2011), pp. 4248–4267.
[18] J.-L. Guermond and Y. Yang, *A Maximum-Principle for Conservation Equations and Consistent Mass Matrix*, submitted.
[19] G.-S. Jiang and E. Tadmor, *Nonoscillatory central schemes for multidimensional hyperbolic conservation laws*, SIAM J. Sci. Comput., 19 (1998), pp. 1892–1917.
[20] S. N. Kružkov, *First order quasilinear equations with several independent variables*, Mat. Sb. (N.S.), 81 (1970), pp. 228–255.
[21] A. Kurganov, G. Petrova, and B. Popov, *Adaptive semidiscrete central-upwind schemes for nonconvex hyperbolic conservation laws*, SIAM J. Sci. Comput., 29 (2007), pp. 2381–2401.
[22] D. Kuzmin, *On the design of general-purpose flux limiters for finite element schemes. I. Scalar convection*, J. Comput. Phys., 219 (2006), pp. 513–531.
[23] D. Kuzmin, R. Löhner, and S. Turek, *Flux–Corrected Transport*, Scientific Computation, Springer, New York, 2005.
[24] D. Kuzmin and S. Turek, *Flux correction tools for finite elements*, J. Comput. Phys., 175 (2002), pp. 525–558.
[25] X.-D. Liu, *A maximum principle satisfying modification of triangle based adaptive stencils for the solution of scalar hyperbolic conservation laws*, SIAM J. Numer. Anal., 30 (1993), pp. 701–716.
[26] A. Logg and G. N. Wells, *DOLFIN: Automated finite element computing*, ACM Trans. Math. Software, 37 (2010), 20.
[27] H. Nessyahu and E. Tadmor, *Nonoscillatory central differencing for hyperbolic conservation laws*, J. Comput. Phys., 87 (1990), pp. 408–463.
[28] L. Piar, F. Babik, R. Herbin, and J.-C. Latché, *A formally second-order cell centred scheme for convection-diffusion equations on general grids*, Internat. J. Numer. Methods Fluids, 71 (2013), pp. 873–890.
[29] R. Sanders, *A third-order accurate variation nonexpansive difference scheme for single nonlinear conservation laws*, Math. Comp., 51 (1988), pp. 535–558.
[30] T. Tezduyar and S. Sathe, *Stabilization parameters in SUPG and PSPG formulations*, J. Comput. Appl. Mech., 4 (2003), pp. 71–88.
[31] T. E. Tezduyar and Y. Osawa, *Finite element stabilization parameters computed from element matrices and vectors*, Comput. Methods Appl. Mech. Engrg., 190 (2000), pp. 411–430.
[32] T. E. Voth, M. J. Martinez, and M. A. Christon, *Generalized Fourier analyses of the advection-diffusion equation—part II: Two-dimensional domains*, Internat. J. Numer. Methods Fluids, 45 (2004), pp. 889–920.
[33] S. T. Zalesak, *Fully multidimensional flux-corrected transport algorithms for fluids*, J. Comput. Phys., 31 (1979), pp. 335–362.
[34] X. Zhang and C.-W. Shu, *On maximum-principle-satisfying high order schemes for scalar conservation laws*, J. Comput. Phys., 229 (2010), pp. 3091–3120.
[35] X. Zhang, Y. Xia, and C.-W. Shu, *Maximum-principle-satisfying and positivity-preserving high order discontinuous Galerkin schemes for conservation laws on triangular meshes*, J. Sci. Comput., 50 (2012), pp. 29–62.
[36] Y. Zhang, X. Zhang, and C.-W. Shu, *Maximum-principle-satisfying second order discontinuous Galerkin schemes for convection-diffusion equations on triangular meshes*, J. Comput. Phys., 234 (2013), pp. 295–316.